Titre: Title:	Optical transmission theory for metal-insulator-metal periodic nanostructures
Auteurs: Authors:	Andre-Pierre Blanchard-Dionne, & Michel Meunier
Date:	2017
Type:	Article de revue / Article
Référence: Citation:	Blanchard-Dionne, A.-P., & Meunier, M. (2017). Optical transmission theory for metal-insulator-metal periodic nanostructures. Nanophotonics, 6(1), 349-355. https://doi.org/10.1515/nanoph-2016-0120

Document en libre accès dans PolyPublie
Open Access document in PolyPublie

URL de PolyPublie: PolyPublie URL:	https://publications.polymtl.ca/4793/
Version:	Version officielle de l'éditeur / Published version Révisé par les pairs / Refereed
Conditions d'utilisation: Terms of Use:	Creative Commons Attribution-Utilisation non commerciale-Pas d'oeuvre dérivée 4.0 International / Creative Commons Attribution-NonCommercial-NoDerivatives 4.0 International (CC BY-NC-ND)

Document publié chez l'éditeur officiel
Document issued by the official publisher

Titre de la revue: Journal Title:	Nanophotonics (vol. 6, no. 1)
Maison d'édition: Publisher:	De Gruyter
URL officiel: Official URL:	https://doi.org/10.1515/nanoph-2016-0120
Mention légale: Legal notice:	

Research article

Open Access

Andre-Pierre Blanchard-Dionne and Michel Meunier*

Optical transmission theory for metal-insulator-metal periodic nanostructures

Abstract: A semi-analytical formalism for the optical properties of a metal-insulator-metal periodic nanostructure using coupled-mode theory is presented. This structure consists in a dielectric layer in between two metallic layers with periodic one-dimensional nanoslit corrugation. The model is developed using multiple-scattering formalism, which defines transmission and reflection coefficients for each of the interface as a semi-infinite medium. Total transmission is then calculated using a summation of the multiple paths of light inside the structure. This method allows finding an exact solution for the transmission problem in every dimension regime, as long as a sufficient number of diffraction orders and guided modes are considered for the structure. The resonant modes of the structure are found to be related to the metallic slab only and to a combination of both the metallic slab and dielectric layer. This model also allows describing the resonant behavior of the system in the limit of a small dielectric layer, for which discontinuities in the dispersion curves are found. These discontinuities result from the out-of-phase interference of the different diffraction orders of the system, which account for field interaction for both inner interfaces of the structure.

Keywords: plasmonics; optics; nanomaterials.

1 Introduction

Surface plasmons are the oscillations of conductive electrons that propagate at the interface of dielectrics and highly conductive metals. They are excited in resonance with electromagnetic waves using momentum matching with the parallel wavevector of the incident wave. With the arrival of fabrication techniques that can achieve resolution well below the wavelength of electromagnetic wave in the visible spectrum, new structures in metals have open up possibilities to couple and manipulate such surface waves [1]. These nano-plasmonic devices have shown to have very unique properties; they can concentrate light well below the diffraction limit [2, 3], they can lead to large field amplification [4], as well as achieve long-range propagation of the surface waves [5]. They constitute a good way of designing materials with unique properties [6, 7], as well as novel optical devices [8, 9].

In this letter, we develop an analytical formalism for a combination of two structures of interest: (i) a metal-insulator-metal (MIM) structure, with (ii) periodic indentation in the metal films, as depicted in Figure 1. Periodic corrugations in metal thin films have shown to exhibit interesting optical properties ever since it was first reported that nanohole arrays lead to extraordinary optical transmission [10]. These structures constitute a unique way to couple to surface waves [11]. As the understanding of the transmission mechanism improved, the high transmission observed in this structure were linked not only to the surface plasmon waves but also to surface waves of the corrugated surface for the case of perfect electrical conductors (PECs) [12]. Planar MIM structures, on their part, have been investigated theoretically for decades now [13] and have gain interest recently with new experimental demonstrations [3, 14, 15] as well as extended analysis for integration into nanoscale devices [16].

The optical properties of such a multilayer structure with periodic corrugation can be obtained using the coupled mode theory. The proposed model includes the calculation of the reflection and transmission coefficient of the interfaces as a semi-infinite medium and a multiple path calculation. This last part corresponds to the combinative solution of a multilayer Fabry-Perot in which one layer acts as a diffraction grating layer. The model is

*Corresponding author: Michel Meunier, Polytechnique Montreal, Montreal, Quebec, Canada, e-mail: michel.meunier@polymtl.ca
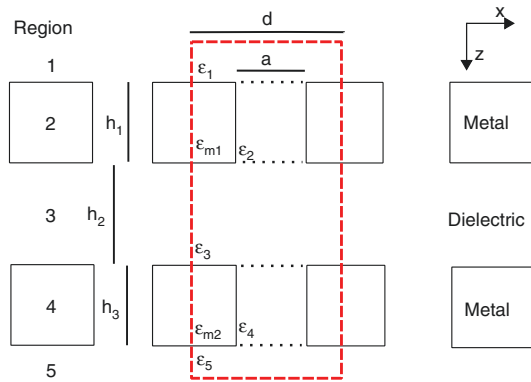Andre-Pierre Blanchard-Dionne: Polytechnique Montreal, Montreal, Quebec, Canada

Figure 1: Unit cell representation of the periodic MIM structure. The dashed rectangle represents the structure with periodicity d; slit width a; and thicknesses h_1, h_2, and h_3 for the top metal, dielectric, and bottom metal layers, respectively.

Figure 2: Field definition for each region of the structure.

developed in order to obtain physical insights into the resonant states involved in the transmission of light through such a structure.

2 Theoretical model

2.1 Scattering coefficients

The theoretical model presented here uses the coupled mode theory in the multiple scattering formalism [17–21]. The structure studied in this paper consists in a dielectric layer of thickness h_2, in between two corrugated metallic layers of thicknesses h_1 and h_3. The periodicity of the system is d and the slit width is a. The dielectric constants of region i are given by ϵ_i (for the metallic layer, this corresponds to the dielectric constant of the material inside the slits), and ϵ_{m_j} for the metals. For simplicity of the method and annotation, as well as for a focus on the interesting case of coupling to surface waves, we consider here only the one-dimensional case of slit arrays, for which the field is invariant along the y-axis, and the p-polarized wave. The metal is considered to be a perfectly flat PEC, but could be implemented as a real metal using surface impedance boundary conditions [21]. The magnetic fields for each layer are defined as solutions to the Helmholtz equation for the considered medium, whether it is a plane wave in a dielectric medium or a guided wave inside the indentation of the metallic layers, as depicted in Figure 2. The notation used for the fields is the one presented in a review article [21] where $|k\rangle = e^{i(k_0 + k_r n)x}$ represents the parallel component (or x-component) of the
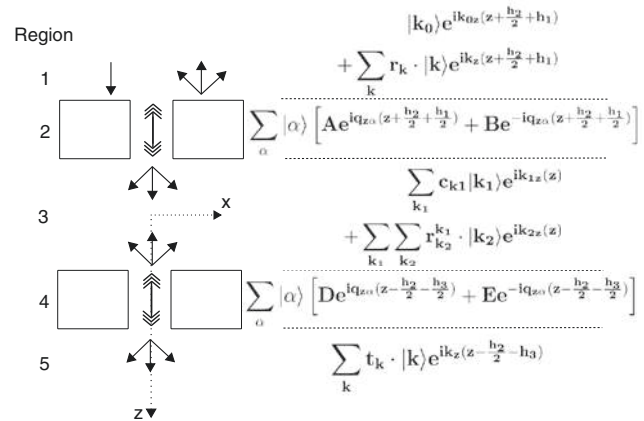
electromagnetic field of a plane wave, with the wavevector $k_{0_i} = k_w \sqrt{\epsilon_i} \sin\theta_i$ with θ_0 the incident angle and $k_w = w/c$ the wavevector of light in free space. The waves in dielectric media are represented by a Bloch combination of plane waves $k = k_0 + k_r n$, which represents the different diffraction orders n of the grating. This representation is valid for an infinite array of slits. For the guided modes inside the slits, $|\alpha\rangle = \dfrac{C_t}{\sqrt{a}}\cos\left(\dfrac{m(x+a/2)}{a}\right)$ represents the parallel component of the guided TM m mode for parallel-plate waveguides [18], where C_t is a normalization constant relative to the waveguide mode and equals 1 if $m = 0$ and $\sqrt{2}$ if $m > 0$. The z-component of the wavevectors is retrieved using $k_w^2 = k^2 + k_z^2$ for the plane wave and $k_w^2 = q_z^2 + (m\pi/a)^2$ for mode m inside the slits.

The transmission and reflection coefficients are obtained, using the convention given in Ref. [21], by matching the fields at each interface and then taking a projection over all $\langle k|$ for the electric fields and over all $\langle \alpha|$ for the magnetic part. This leads to a set of equations for each interface, as follows:

1. Interface 1–2

$$(G_{\alpha\alpha} + iY_\alpha)\tau_\alpha^{12} + \sum_{\alpha \neq \beta} G_{\alpha\beta}\tau_\beta^{12} = 2iY_{k0}\langle k_0|\alpha\rangle, \tag{1}$$

$$\rho_{k_1}^{12} = -\delta_{k_0,k_1} + \sum_\alpha \langle k_1|\alpha\rangle \tau_{\alpha,k_1}^{12}, \tag{2}$$

2. Interface 2–3

$$(G_{\gamma\gamma} + iY_\gamma)\rho_{\alpha\gamma}^{23} + \sum_{\beta \neq \gamma} G_{\alpha\beta}\rho_{\alpha\beta}^{23} = iY_\gamma \delta_{\gamma\alpha} - G_{\gamma\alpha}, \tag{3}$$

$$\tau_{\alpha,k}^{23} = \langle k|\alpha\rangle + \sum_\beta \rho_{\alpha\beta}^{23}\langle k|\beta\rangle, \tag{4}$$

3.   Interface 3–4

$$(G_{\alpha\alpha} + iY_\alpha)\tau^{34}_{\alpha,k} + \sum_{\alpha \neq \beta} G_{\alpha\beta}\tau^{34}_{\beta,k} = 2iY_k\langle k|\alpha\rangle, \qquad (5)$$

$$\rho^{34}_{k_1,k_2} = -\delta_{k_1,k_2} + \sum_\alpha \langle k_2|\alpha\rangle\tau^{34}_{\alpha,k_1}, \qquad (6)$$

where τ^{12}_α represents the transmission coefficient for interface 1–2 of mode α, and $Y_k = \epsilon_i k_w/k_z$ represents the admittance of p-polarized wave. $Y_\alpha = q_z/k_w$ is the admittance of the TM mode inside the slit. $\rho^{23}_{\alpha\gamma}$ represents the reflection coefficient of mode α into mode γ, and $\tau^{34}_{\alpha,k}$ represents the transmission into mode α of incoming k wavevector. $G_{\alpha\alpha} = i\sum_k Y_k\langle k|\alpha\rangle\langle\alpha|k\rangle$ describes the coupling term of incident wave to the waveguide mode α with plane vectors $|k\rangle$, and must run over a sufficient number of diffraction orders. It includes, for each wavevector, the overlap integral for one-dimensional slit arrays:

$$\langle k|\alpha\rangle = \frac{C_t}{\sqrt{ad}}\int_{-a/2}^{a/2}\cos(m\pi a(x+a/2))e^{(ikx)}dx$$
$$= \frac{C_t ik}{\sqrt{ad}}\frac{e^{ika/2}\cos(m\pi) - e^{-ika/2}}{(m\pi/a)^2 - k^2}. \qquad (7)$$

The reflection and transmission terms for all the other interfaces can be retrieved by applying Eqs. (1)–(6) in a similar way. In region 3, the waves are represented by a superposition of incoming diffraction orders and reflected ones, denoted by k_1, k_2.

2.2 Multiple path calculation

Because of the difference of impedance of each medium involved in the MIM structure, the waves that propagate inside this structure will experience multiple reflections and transmissions at each interface. These reflections can occur an infinite number of times, and their summation is represented by a geometric series. Transmission "loops" can be defined inside the structure in order to enumerate every possible path of light inside the structure. In a multilayer system like the MIM structure, each layer and combination of layers will behave as a possible "loop" of the transmission. Figure 3 represents the different loops possible in the four-interface MIM structure.

The total transmission becomes a complex summation of all possible paths, which will define how the fields inside each layer interact with each other. Light can be transmitted directly, as represented by the t^d arrow in Figure 3, or can go through a series of loops of the system before being transmitted. Loops can also exist inside other loops.

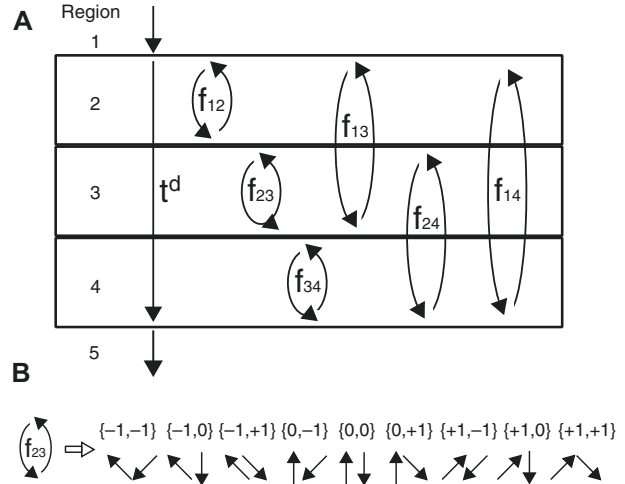Waves inside the slits can propagate as different modes of the parallel plate waveguide, so all possible

Figure 3: (A) The different loops inside the MIM structure. (B) The expansion of loop f_{23} by taking into account the first diffraction orders.

loops containing these regions can be expanded into the different combinations of the guided modes considered. Furthermore, plan waves in region 3 can propagate as diffraction orders of the periodic system, as described by the indices of the reflection and transmission coefficients $\tau^{34}_{\alpha,k}$, $\tau^{23}_{\alpha,k}$, $\rho^{34}_{k_1,k_2}$, and $\rho^{32}_{k_1,k_2}$. Every loop containing this region, i.e. f_{23}, f_{13}, f_{24}, and f_{14}, must be expanded into combinations of diffraction orders both coming back and forth. In Figure 3B, an example of the different loop combination of f_{23} is given for orders $-1, 0, +1$.

In this calculation, a sufficient number of diffraction orders and guided modes must be taken into consideration. Whenever $\sqrt{\epsilon_i}k_w\sin(\theta) + \frac{m2\pi}{d} < k_w\sqrt{\epsilon_i}$, the diffraction order inside the medium becomes evanescent, and so the term e_h will become significantly small. As for the guided modes, as only the fundamental mode for the metallic slits couples strongly to the plane waves of regions 1, 3, and 5, only this mode is considered for the remainder of the article. The loop factors, with diffraction order (-1, 0, $+1$) considered for region 3 and only the transverse electric and magnetic (TEM)-guided mode considered in regions 2 and 4 ($\rho^{23}_{|0\rangle,|0\rangle}$ is written ρ^{23}), can be expressed as

$$f^{12} = \rho^{23}\rho^{21}e^2_{h_1} \quad f^{34} = \rho^{45}\rho^{43}e^2_{h_3}$$
$$f^{23}_{k_1,k_2} = \rho^{34}_{k_1,k_2}\rho^{32}_{k_2,k_1}e_{h_2}(k_1)e_{h_2}(k_2)$$
$$f^{13}_{k_1,k_2} = \rho^{34}_{k_1,k_2}\tau^{32}_{k_2}\rho^{21}\tau^{23}_{k_1}e^2_{h_1}e_{h_2}(k_2)e_{h_2}(k_1)$$
$$f^{24}_{k_1,k_2} = \rho^{45}\tau^{43}_{k_1}\rho^{32}_{k_1,k_2}\tau^{34}_{k_2}e_{h_2}(k_2)e_{h_2}(k_1)e^2_{h_3}$$
$$f^{14}_{k_1,k_2} = \rho^{45}\tau^{43}_{k_1}\tau^{32}_{k_1}\rho^{21}\tau^{23}_{k_2}\tau^{34}_{k_2}e_{h_2}(k_2)e_{h_2}(k_1)e^2_{h_1}e^2_{h_3}, \qquad (8)$$

where k_1 is the parallel wavevector of light going forward and k_2 is the one going backward, $e_{h_2}(k) = e^{iq_z h_2}$ represents

the propagation term inside the dielectric layer, and $e_{h_j} = e^{ik_{k_{z_j}} h_j}$ the one for the metallic layers. The direct transmission of light in the structure is represented by

$$t_k^d = \tau^{12} \tau_k^{23} \tau_k^{34} \tau^{45} e_{h_1} e_{h_2}(k) e_{h_3}, \tag{9}$$

with k wavevector inside the dielectric layer. The total transmission coefficient is given by

$$t = \sum_k t_k^d (1 + A_{14}), \tag{10}$$

where A_{14} represents the considered summation of every possible combination of loops of the system. This is achieved using the following matrix form:

$$A_{14} = \mathbf{V}_k^{in} \times [\mathbf{I} - \mathbf{T}_k]^{-1} \times \mathbf{V}_k^{out}, \tag{11}$$

where $\mathbf{V}_k^{in}$ is a vector representing the initial loop of a certain combination, $\mathbf{I}$ is the identity matrix, $\mathbf{T}_k$ is a matrix of a subsequent loop with the corresponding connecting coefficient, and $\mathbf{V}_k^{out}$ represents the exit coefficient of the final loop considered. The middle term in Eq. (11) is a geometric series of matrices that sums up all possible combination of paths, in the same way a simple geometric series sums up all paths of a single layer. These vectors and matrices take the form

$$\mathbf{V}_k^{in} = [a^{12} f^{12} a_{k1,k2}^{23} f_{k1,k2}^{23}, \ldots, a_{k1,k2}^{14} f_{k1,k2}^{14t}], \tag{12}$$

$$\mathbf{T}_k = \begin{bmatrix} a^{12-12} f^{12} & a_{k1,k2}^{12-23} f_{k1,k2}^{23} & \cdots & a_{k1,k2}^{12-14} f_{k1,k2}^{14t} \\ a^{23-12} f^{12} & a_{k1,k2}^{23-23} f_{k1,k2}^{23} & \cdots & a_{k1,k2}^{23-14} f_{k1,k2}^{14t} \\ \vdots & \vdots & \ddots & \vdots \\ a^{14-12} f^{12} & a_{k1,k2}^{14-23} f_{k1,k2}^{23} & \cdots & a_{k1,k2}^{14-14} f_{k1,k2}^{14t} \end{bmatrix}, \tag{13}$$

$$\mathbf{V}_k^{out} = [t_{k_2}^{12} \quad t_{k_2}^{23} \quad \cdots \quad t_{k_2}^{14}]^T, \tag{14}$$

where $a_{k1,k2}^{xy-ab}$ represents a connecting coefficient that uses the previous wavevector k_1 as the incoming wavevector for the reflection coefficient of the next loop. The exit coefficient $t_{k_2}^{23}$ inputs the correct transmission coefficient for the considered path, using the wavevector of the last loop. It is to be noted that the vectors and matrices of Eqs. (12) and (13) use the loop factors f_{13t}, f_{24t}, and f_{25t}, which consider the loop with a summation of the previous possible loop that can exist inside. Finer details are provided in the Supplementary Information section. The total transmission of the system is given by $T = |t|^2$. A Matlab code for the implementation of the model is available in the Supplementary Information section.

3 Results

3.1 Transmission in the subwavelength regime with a thick dielectric layer

In Figure 4, the transmission spectra of a nanostructured MIM is presented for the case of PEC and dielectric constant $\epsilon_1 = \epsilon_2 = \epsilon_3 = 1$. The dimensions, relative to the period of the system d, are $h_1 = h_3 = 2d$, $h_2 = 1.6d$, $a = 0.25d$. The curves obtained for the transmission spectrum of this structure with a finite element simulation via the COMSOL software is superposed and shows perfect agreement. The time of calculation is 10^2 faster with the model for a similar resolution on the number of wavelength steps. This improvement in calculation time rises to 10^3 when only the zero diffraction order is considered inside the dielectric layer (which is valid in the subwavelength regime for thick dielectric layers). In the case of a two-dimensional structure calculation, this improvement factor would rise to another 10-fold.

The transmission is characterized by a series of resonant peaks spaced apart in multiples of the length of the different cavities of the structure. As no radiative losses from the surface roughness of the layer as well as no absorption losses from the metal are included in the model, full transmission ($T = 1$) is reached for resonant wavelengths. In the lower panel, the phase term associated with the wave propagation of loop f_{12} and f_{13t} is represented. This phase term is obtained by using $\phi = \text{atan}$
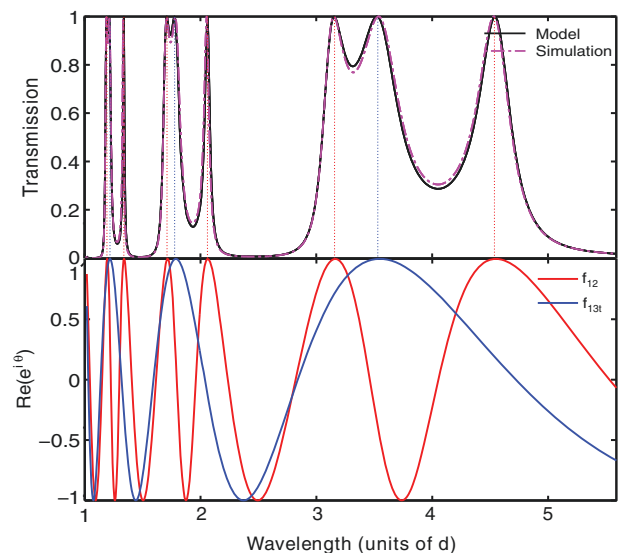

Figure 4: Transmission of the MIM periodic structure for dimensions $a = 0.25d$, $h_1 = h_3 = 1.6d$, and $h_2 = 2d$.

($Im(f)/Re(f)$). It includes both the phase shift from the optical propagation and the phase shift resulting from the reflection on the interface, and for f_{12} this is given by $\phi = \phi_1 + \phi_2$, where $\phi_1 = q_{z\alpha}h_1$ and $\phi_2 = \mathrm{atan}(Im(\rho)/Re(\rho))$. The loop $f_{13t} = \dfrac{f_{13}}{(1-f_{12})(1-f_{23})}$ represents the loop of the combination of layers 1 and 2, with the geometric summation of the inner loops f_{12} and f_{23} included. The resonances of the system occurs when $\mathrm{Real}(e^{i2\phi}) = 1$ for both loops. This condition for loop f_{12} means that modes from the metallic layer individually can emerge as a resonant state of the system. The other resonances occur for a combination of both the metallic layer and the dielectric layer (loop f_{13t}). No resonance from the dielectric layer only is observed, which is consistent with the fact that light needs to travel through the metallic layer first, which only allows resonant modes to go through.

In Figure 5, the dispersion curves of the structure are represented, with the $\mathrm{Real}(e^{i2(\phi_1+\phi_2)}) = 1$ condition represented by the black dashed line for the f_{12} modes and gray dashed lines for the f_{13t} modes. For a small incident wavevector, the resonances associated with the metallic layer behave like Fabry-Perot cavity modes with no dependence over the tangential wavevector component k_x [18] as the propagation vector for this loop is given by the TEM mode of the slits $q_z = k_w$. The modes of f_{13t} behave as dielectric core and metallic cladding waveguide modes, but phase shifted as it includes a propagation inside the metallic slit as well as the propagation inside the dielectric bounded by metallic layers. A remarkable bending of all curves occurs close to the "folding" of the light line, which is a well-known feature of periodic corrugation inside a metallic film [12]. This bending is connected to the

coupling to modes of the corrugated surface and is represented through the admittance of the modes reaching high values close to the Wood anomaly condition $k_z = 0$ [12]. The resonant state can thus be described as having either a cavity-like character (ϕ_1) or a surface mode character (ϕ_2) [21, 22], depending on which phase factor is contributing more to the resonance.

3.2 Transmission in the subwavelength regime with a thin dielectric layer

In the subwavelength regime considered throughout this paper, the diffraction orders inside the dielectric are evanescent. They will only contribute significantly to the total transmission when the dielectric layer is decreased to a size where the exponential decay is small. The resonances in this case emerge from the summation of the contribution of every diffraction order. Such a situation is represented in the dispersion graph of Figure 6. The curves in panel A show resonances relative to a MIM structure with dimensions $h_1 = h_3 = 1.6d$, $a = 0.2d$, $h_2 = 0.5d$. An important property to observe from this graph is the discontinuities in the resonant behavior of the system, reminiscent of bandgaps in the dispersion relation of planar MIM structure [16]. The transmission coefficient for the direct transmission term with (B) $k = k_0$ and (C) $k = k_0 - k_r$ wavevectors are plotted in the subpanel (the transmission factor for the $+1$ diffraction order is negligible). These graphs show the transmission coefficient reaching values close to 1 and -1 near the same region, which indicate resonant states that are out of phase with one another, leading to no field being transmitted through the total structure. This direct transmission factor includes the interaction term of the field localized at both surfaces, which influences their respective propagation, as in a planar MIM structure.

In conclusion, a MIM structure presents resonant behavior that resembles a combination of the modes of a corrugated metallic film with the Fabry-Perot modes of a dielectric layer. These modes can in fact be described using the phase condition of unity for a loop containing both layers, as well as modes of the loop of the metallic layer only. When the evanescent higher-order diffraction modes inside the dielectric become considerable, the surface fields on both surfaces influence the resonance behavior of the system, as in a MIM structure. Destructive interference from these fields creates discontinuity in the dispersion curves where no transmission is observed.
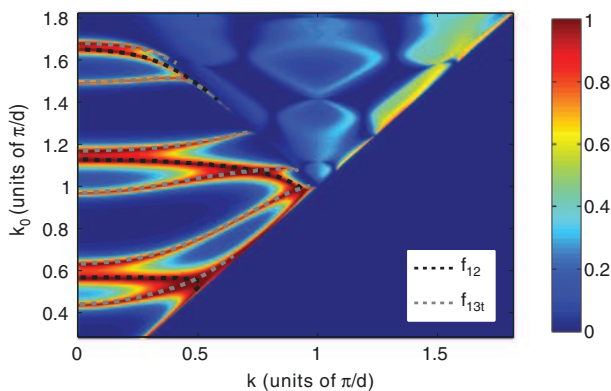
Figure 5: Dispersion curves of the MIM structure with dimensions $h_1 = h_3 = 1.6d$, $a = 0.25d$, and $h_2 = 2d$. The dashed black line represents the resonance condition for the f_{12} loop and the gray dashed line for the f_{13t} loop.
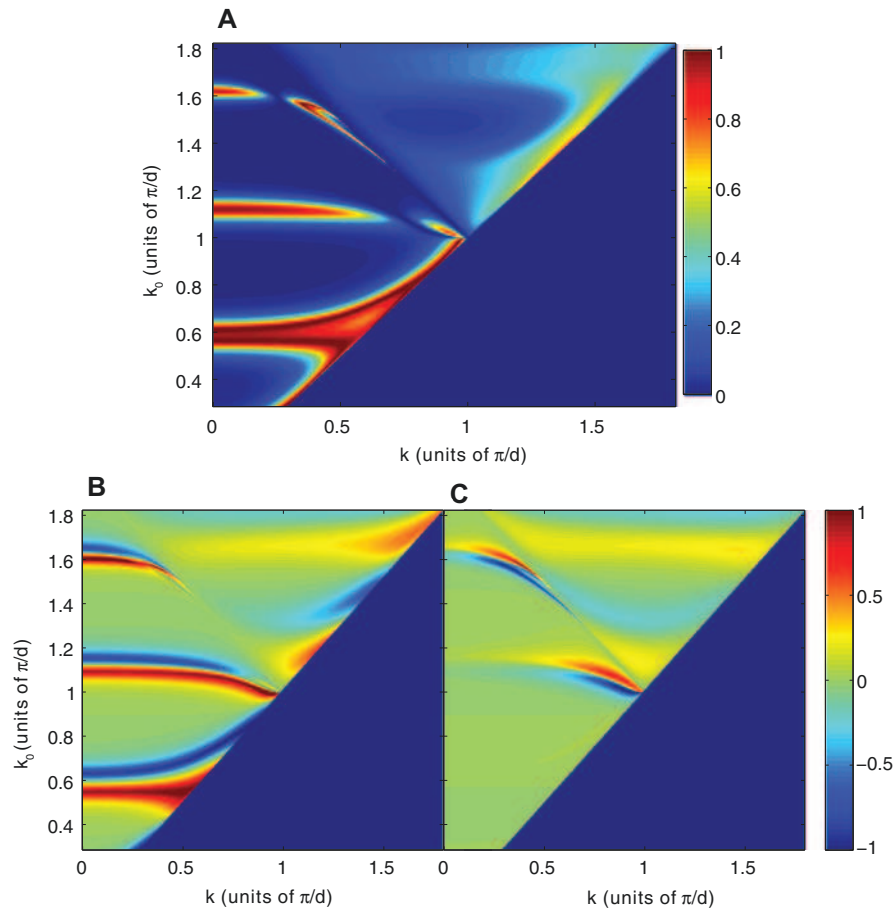
Figure 6: (A) Dispersion relation for MIM structure with $h_1 = h_3 = 1.6d$, $a = 0.25d$, and $h_2 = 0.5d$. Discontinuities in the dispersion curves can be found for the upper branches. Subpanel: transmission coefficient with diffraction order (B) 0 and (C) −1 considered for the direct transmission term t^d.

References

[1] Barnes WL, Dereux A, Ebbesen TW. Surface plasmon subwavelength optics. Nature 2003;424:824–30.

[2] Gramotnev DK, Bozhevolnyi SI. Plasmonics beyond the diffraction limit. Nat Photon 2010;4:83–91.

[3] Choo H, Kim MK, Staffaroni M, et al. Nanofocusing in a metal-insulator-metal gap plasmon waveguide with a three-dimensional linear taper. Nat Photon 2012;6:838–44.

[4] Schuller JA, Barnard ES, Cai W, Jun YC, White JS, Brongersma ML. Plasmonics for extreme light concentration and manipulation. Nat Mater 2010;9:193–204.

[5] Oulton RF, Sorger VJ, Genov DA, Pile DFP, Zhang X. A hybrid plasmonic waveguide for subwavelength confinement and long-range propagation. Nat Photon 2008;2:496–500.

[6] Shen JT, Catrysse PB, Fan S. Mechanism for designing metallic metamaterials with a high index of refraction. Phys Rev Lett 2005;94:197401.

[7] Shalaev VM. Optical negative-index metamaterials. Nat Photon 2007;1:41–8.

[8] Drezet A, Genet C, Ebbesen TW. Miniature plasmonic wave plates. Phys Rev Lett 2008;101:043902.

[9] Ferry VE, Sweatlock LA, Pacifici D, Atwater HA. Plasmonic nanostructure design for efficient light coupling into solar cells. Nano Lett 2008;8:4391–7.

[10] Ebbesen TW, Lezec HJ, Ghaemi HF, Thio T, Wolff PA. Extraordinary optical transmission through sub-wavelength hole arrays. Nature 1998;391:667.

[11] Genet C, Ebbesen TW. Light in tiny holes. Nature 2007;445:39–46.

[12] Pendry JB, Martin-Moreno L, Garcia-Vidal FJ. Mimicking surface plasmons with structured surfaces. Science 2004;305:847–8.

[13] Economou EN. Surface plasmons in thin films. Phys Rev 1969;182:539.

[14] Kurokawa Y, Miyazaki HT. Metal-insulator-metal plasmon nanocavities: analysis of optical properties. Phys Rev B 2007;75:035411.

[15] Hill MT, Marell M, Leong ESP, et al. Lasing in metal-insulator-metal sub-wavelength plasmonic waveguides. Optics Express 2009;17:11107–12.

[16] Dionne JA, Sweatlock LA, Atwater HA, Polman A. Planar metal plasmon waveguides: frequency-dependent dispersion, propagation, localization, and loss beyond the free electron model. Phys Rev B 2005;72:075405.

[17] Martin-Moreno L, Garcia-Vidal FJ, Lezec HJ, et al. Theory of extraordinary optical transmission through subwavelength hole arrays. Phys Rev Lett 2001;86:1114.

[18] Bravo-Abad J, Martin-Moreno L, Garcia-Vidal FJ. Transmission properties of a single metallic slit: from the subwavelength regime to the geometrical-optics limit. Phys Rev E 2004;69:026601.

[19] Garcia-Vidal FJ, Martin-Moreno L. Transmission and focusing of light in one-dimensional periodically nanostructured metals. Phys Rev B 2002;66:155412.

[20] Martin-Moreno L, Garcia-Vidal FJ. Minimal model for optical transmission through holey metal films. J Phys Condens Matter 2008;20:304214.

[21] Garcia-Vidal FJ, Martin-Moreno L, Ebbesen TW, Kuipers L. Light passing through subwavelength apertures. Rev Modern Phys 2010;82:729.

[22] Marquier F, Greffet JJ, Collin S, Pardo F, Pelouard JL. Resonant transmission through a metallic film due to coupled modes. Opt Express 2005;13:70–6.